Hertz-Level Measurement of the Optical Clock Frequency in a Single $^{88}Sr^{+}$ Ion

H. S. Margolis *et al.*

Science **306**, 1355 (2004);
DOI: 10.1126/science.1105497

Science (print ISSN 0036-8075; online ISSN 1095-9203) is published weekly, except the last week in December, by the American Association for the Advancement of Science, 1200 New York Avenue NW, Washington, DC 20005.

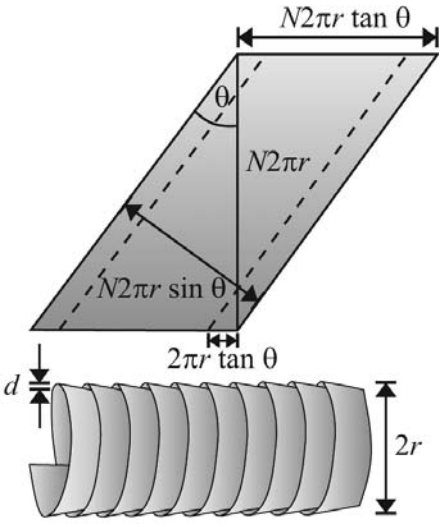

Fig. 3. Design for a chiral material. Continuous insulated strips of metal are wound in a helix and then individual coils are stacked in a three-dimensional log pile to make an isotropic structure.

winding a continuous insulated metal tape onto a cylinder so that it forms an overlapping helix (Fig. 3). More details of the performance of this structure are available (figs. S8 to S13). This is a chiral variant of the so-called Swiss roll structure used to produce negative permeability in the MHz range of frequencies (*14*). The structure is resonant because of inductance in the coiled helix and capacitance between the inner and outer layers of the helix. When current flows along the helix, not only does it produce a magnetic polarization along the axis, but it also produces an electric polarization because some of the current flows parallel to the axis. Typical values for the parameters are

$$r = 5 \times 10^{-3}\ \text{m}$$
$$a = 2 \times 10^{-2}\ \text{m},\ d = 1 \times 10^{-4}\ \text{m}$$
$$\theta = 5^\circ,\ N = 10 \qquad (12)$$

where a is the lattice constant of the log-pile structure and r, d, θ, and N are defined in Fig. 3. These parameters give negative refraction at around 100 MHz. The design can be tuned over a wide range of frequencies (SOM Text). Achieving strong chirality in the optical region of the spectrum is more difficult, but some promising design studies have been made (*15*).

The class of negatively refracting materials introduced here with the prescribed properties should open previously unknown avenues of investigation. Specific designs are greatly simplified with very compact internal structure, typically on a scale less than 1/100th of the free space wavelength at the resonant frequency. The structures offer further opportunities to extend the negative refraction concept.

References and Notes

1. J. B. Pendry, *Phys. Rev. Lett.* **85**, 3966 (2000).
2. J. B. Pendry, S. A. Ramakrishna, *J. Phys. Cond. Matter* **15**, 6345 (2003).
3. D. R. Smith, J. B. Pendry, M. C. K. Wiltshire, *Science* **305**, 788 (2004).
4. V. G. Veselago, *Soviet Physics Usp.* **10**, 509 (1968).
5. J. B. Pendry, A. J. Holden, W. J. Stewart, I. Youngs, *Phys. Rev. Lett.* **76**, 4773 (1996).
6. J. B. Pendry, A. J. Holden, D. J. Robbins, W. J. Stewart, *IEEE Trans. Microwave Theory Tech.* **47**, 2075 (1999).
7. D. R. Smith, W. J. Padilla, D. C. Vier, S. C. Nemat-Nasser, S. Schultz, *Phys. Rev. Lett.* **84**, 4184 (2000).
8. A. A. Houck, J. B. Brock, I. L. Chuang, *Phys. Rev. Lett.* **90**, 137401 (2003).
9. A. Grbic, G. V. Eleftheriades, *Phys. Rev. Lett.* **92**, 117403 (2004).
10. P. V. Parimi *et al.*, *Phys. Rev. Lett.* **92**, 127401 (2004).
11. E. Cubukcu, K. Aydin, E. Ozbay, S. Foteinopoulou, C. M. Soukoulis, *Nature* **423**, 604 (2003).
12. P. V. Parimi, W. T. Lu, P. Vodo, S. Sridhar, *Nature* **426**, 404 (2003).
13. E. Cubukcu, K. Aydin, E. Ozbay, S. Foteinopolou, C. M. Soukoulis, *Phys. Rev. Lett.* **91**, 207401 (2003).
14. M. C. K. Wiltshire *et al.*, *Science* **291**, 849 (2001).
15. Y. Svirko, N. Zheludev, *Appl. Phys. Lett.* **78**, 498 (2001).
16. I thank the Donostia International Physics Center (DIPC) for their hospitality during the course of this work; the Engineering and Physical Sciences Research Council for a senior fellowship; and the European Commission (EC) under project FP6-NMP4-CT-2003-505699, the U.S. Department of Defense/Office of Naval Research Multidisciplinary University Research Initiative grant N00014-01-1-0803, and the EC Information Societies Technology (IST) program Development and Analysis of Left-Handed Materials (DALHM) project number IST-2001-35511 for financial support.

Supporting Online Material
www.sciencemag.org/cgi/content/full/306/5700/1353/DC1
SOM Text
Figs. S1 to S13

15 June 2004; accepted 1 September 2004

Hertz-Level Measurement of the Optical Clock Frequency in a Single $^{88}Sr^{+}$ Ion

H. S. Margolis,* G. P. Barwood, G. Huang, H. A. Klein, S. N. Lea, K. Szymaniec, P. Gill

The frequency of the 5s $^2S_{1/2}$–4d $^2D_{5/2}$ electric quadrupole clock transition in a single, trapped, laser-cooled $^{88}Sr^{+}$ ion has been measured by using an optical frequency comb referenced to a cesium fountain primary frequency standard. The frequency of the transition is measured as 444,779,044,095,484.6 (1.5) hertz, with a fractional uncertainty within a factor of 3 of that of the cesium standard. Improvements required to obtain a cesium-limited frequency measurement are described and are expected to lead to a $^{88}Sr^{+}$ optical clock with stability and reproducibility exceeding that of the primary cesium standard.

Accurate time and frequency measurement is a long-standing requirement of science and technology, with applications including the realization of the Système International (SI) base units of time and length, satellite-based navigation and ranging, precision measurements of fundamental constants, and tests of physical theories (*1*). Since 1967, the internationally agreed definition of the second has its basis in the ground-state hyperfine transition in the ^{133}Cs atom at 9,192,631,770 Hz, and Cs fountain primary frequency standards now have reproducibilities of around 1 part in 10^{15} (*1*). Recent studies have indicated the potential of optical frequency standards based on high-Q transitions in laser-cooled trapped ions or atoms to achieve even better stabilities and accuracies (*2*, *3*). Combined with optical frequency measurement techniques based on femtosecond combs (*4*, *5*), these transitions may be used as practical frequency standards generating a direct microwave output (*3*), raising the possibility of a future redefinition of the SI second. To assess the suitability of an optical standard as the basis for such a new definition, it is important to make accurate measurements of its frequency relative to the Cs standard and to evaluate its reproducibility. In the medium term, this would allow such standards to be used as secondary representations of the second, contributing to International Atomic Time (TAI).

An important class of optical frequency standards are those that have their basis in narrow-linewidth forbidden transitions in single laser-cooled trapped ions, such as $^{199}Hg^{+}$ (*2*), $^{171}Yb^{+}$ (*6*, *7*), $^{115}In^{+}$ (*8*), and $^{88}Sr^{+}$ (*9*, *10*). The best previously reported frequency measurements are for the $^{199}Hg^{+}$ standard at 282 nm (*11*) and the $^{171}Yb^{+}$ standard at 435 nm (*6*), with quoted uncertainties of 1 part in 10^{14}. We present a measure-

National Physical Laboratory (NPL), Teddington, Middlesex TW11 0LW, UK.

*To whom correspondence should be addressed. E-mail: helen.margolis@npl.co.uk

ment of the 5s $^2S_{1/2}$–4d $^2D_{5/2}$ optical clock transition frequency in $^{88}Sr^+$ at 674 nm, with a fractional uncertainty that is three times better than the previous best measurements.

A partial term diagram for the $^{88}Sr^+$ optical frequency standard is shown (Fig. 1A). The ion is trapped in an endcap trap (*12*) and laser-cooled to a few mK on the 5s $^2S_{1/2}$–5p $^2P_{1/2}$ transition at 422 nm. To prevent optical pumping into the metastable 4d $^2D_{3/2}$ state, we used 1092-nm laser radiation. Fluorescence from the 422-nm cooling transition is detected by a photomultiplier tube, and the micromotion of the ion is monitored and minimized in three dimensions by using radio frequency (rf)–photon correlation techniques (*13*, *14*). The reference for the optical frequency standard is the 5s $^2S_{1/2}$–4d $^2D_{5/2}$ electric quadrupole transition at 674 nm, which has a natural linewidth of 0.4 Hz. This is probed with the use of a 674-nm extended-cavity diode laser, which is stabilized to a high-finesse ultra-low-expansion (ULE) cavity by using the Pound-Drever-Hall technique (*15*), resulting in a laser linewidth of less than 100 Hz and a relative frequency stability of $1\times10^{-14}/\sqrt{\tau}$ for averaging times $\tau < 10$ s. The frequency-stabilized probe laser is shifted into resonance with the 674-nm clock transition frequency by using a double-passed acousto-optic modulator (AOM). The clock transition is observed by using the quantum jump technique (*16*); i.e., excitation to the metastable 4d $^2D_{5/2}$ level is detected from cessation of the strong 422-nm fluorescence from the cooling transition.

In a dc magnetic field (typically 1.4 μT), the clock transition splits into 10 Zeeman components (Fig. 1B). The $^{88}Sr^+$ ion is interrogated by using a computer-controlled sequence of operations during which the ion is alternately cooled at 422 nm and then probed at 674 nm. The probe laser pulses were typically 5 ms in duration, resulting in a Fourier transform–limited linewidth of about 200 Hz. The center frequency, ν_0, of the Zeeman structure is determined by using a four-point servo scheme with a typical cycle time of 15 to 20 s to probe a pair of Zeeman components, which are symmetrically placed around line center (*17*).

Absolute frequency measurements of the clock transition frequency were performed by simultaneously recording the AOM offset frequency and measuring the frequency of the light locked to the ULE cavity with the use of a femtosecond optical frequency comb. The setup of this frequency comb was similar to that described in (*9*), except that both the repetition rate and the carrier envelope offset frequency were stabilized to rf synthesizers referenced to the 10-MHz output of a hydrogen maser. The offset of the maser output frequency from 10 MHz was determined by comparison with the NPL Cs fountain (*18*) throughout the period of the frequency measurements. The stability of the rf synthesizers used on the comb contributes to the statistical uncertainty of the frequency measurements, but the comb linkage does not significantly affect the final systematic uncertainty.

The largest source of systematic frequency shift for the $^{88}Sr^+$ optical frequency standard arises from the electric quadrupole shift of the reference transition (*17*), which is due to the interaction between the electric quadrupole moment of the atomic states and any residual electric field gradient present at the position of the ion. After the treatment in (*19*), the resultant frequency shift of the 4d $^2D_{5/2}$ level with magnetic quantum number m_j' (j indicates total angular movement) is given by

$$\Delta\nu = \frac{3}{10h} Q_{dc}\Theta(D,5/2) \times \left(\frac{35}{12} - m_j'^2\right)(3\cos^2\beta - 1) \qquad (1)$$

where Q_{dc} is the residual dc quadrupole field gradient at the position of the ion, $\Theta(D,5/2)$ is the electric quadrupole moment of the 4d $^2D_{5/2}$ state, β is the angle between the principal axis of the quadrupole field gradient and the magnetic field axis, and h is Planck's constant. The 5s $^2S_{1/2}$ state has no electric quadrupole moment and so is not shifted by this effect. The residual dc quadrupole field gradient is determined from measurements of the trap secular frequencies and minimized by adjusting the dc voltages applied to the outer electrodes of the endcap trap (*17*). In this way the shift is reduced to the level of a few Hz. However, the quadrupole shift can be nulled by using one of two different techniques, with the result that the uncertainty in this shift can be reduced to a substantially lower level. In the first, referred to as method A, a particular pair of Zeeman components is selected, and frequency measurements are carried out for three mutually orthogonal orientations of the applied dc magnetic field. The average quadrupole shift for these three measurements is zero (*19*). In the second technique (method B), measurements are carried out by using three different pairs of Zeeman components that correspond to transitions with the three different possible values of $|m_j'|$, for example, pairs a, b, and c in Fig. 1B (*10*, *20*). From Eq. 1, the average quadrupole shift for these three transitions is again zero, independent of the magnetic field direction.

Frequency measurements of the 5s $^2S_{1/2}$–4d $^2D_{5/2}$ transition in $^{88}Sr^+$ were carried out on 11 separate days. The first 6 days of data (Fig. 2A) were taken with the use of method A to null the electric quadrupole shift, with measurements being carried out in three nominally orthogonal magnetic field directions corresponding to angles of β of about 11°, 101°, and 90°. The later 5 days of data (Fig. 2B) were taken with the use of method B to null the electric quadrupole shift. For 2 of these days, the magnetic field direction was such that $\beta \approx 11°$; for the other 3 days, β was about 90°. Each data point corresponds to typically 10,000 s of data, and the error bars represent statistical uncertainties only. The unweighted mean frequencies of the two sets of data (before correcting for systematic errors) are 444,779,044,095,485.0 (1.3) Hz and 444,779,044,095,486.2 (1.2) Hz, respectively, where the statistical standard uncertainties are shown in parentheses.

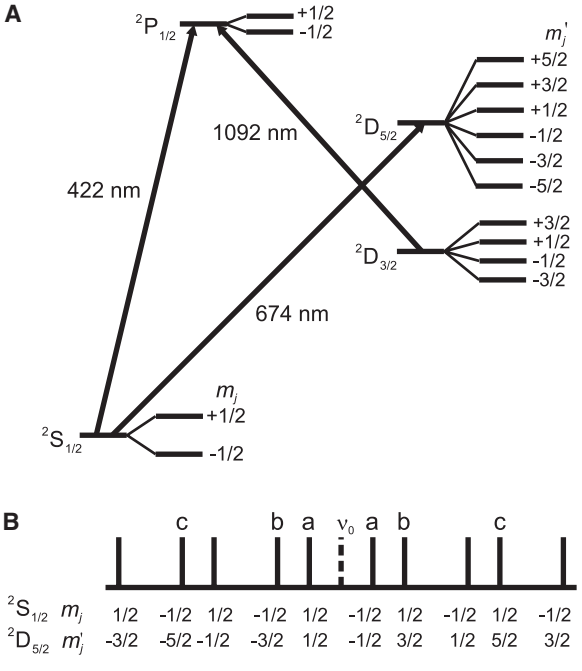

Fig. 1. (**A**) Partial term scheme for $^{88}Sr^+$ (nuclear spin $I = 0$), showing the transitions used to cool and probe the trapped ion. (**B**) Zeeman splitting of the 5s $^2S_{1/2}$–4d $^2D_{5/2}$ clock transition, showing the m_j quantum numbers for each component and the centroid ν_0 of the multiplet.

A detailed analysis of ion-related systematic errors for the $^{88}Sr^{+}$ optical frequency standard was presented in (*10*). The estimated sizes of these effects for our system are given in Table 1 together with some technical sources of systematic uncertainty, the effects of which have been evaluated experimentally wherever possible.

Although the quadrupole shift of the transition frequency is nominally nulled for both sets of data, the cancellation of the shift in method A requires the three magnetic field orientations to be exactly orthogonal. Allowing for an estimated 10° of uncertainty in the magnetic field directions chosen, the residual uncertainty due to the quadrupole shift is estimated to be around 10% of the mean magnitude of the shift. The cancellation of the quadrupole shift in method B relies only on the angle between the magnetic field axis and the quadrupole axis being stable over the course of a day's measurements, and so the residual uncertainty is assumed to be negligible in this case.

The thermal secular motion of the trapped ion and the micromotion at the trap drive frequency both lead to Stark shifts (which arise because the ion experiences a nonzero time-averaged value of the ac trapping field) and to second-order Doppler shifts. The shifts arising from the micromotion are estimated from the rf photon correlation signals (*14*), whereas those due to the secular motion are estimated from the intensity of the secular sidebands relative to the carrier. There is also a Stark shift arising from blackbody radiation, if the transition frequency is corrected to absolute zero. At 293 K, this is calculated to be 0.30 (8) Hz (*10*), with the uncertainty arising primarily from the uncertainty in the Stark shift coefficients.

The linear Zeeman effect is eliminated by probing two Zeeman components, which are symmetrically placed around line center. The quadratic Zeeman effect shifts both components in the same direction but, at the typical dc applied magnetic field of about 1.4 μT, is negligible compared to other sources of uncertainty. The blackbody radiation field, with a mean-square magnetic field amplitude of 7.01 μT^2 at 293 K, and ac magnetic fields similarly lead to negligible Zeeman shifts at the current level of precision.

The radiation used to cool and probe the trapped ion can cause ac Stark shifts of the clock transition frequency. The procedures used to null the electric quadrupole shift also null the tensor component of these ac Stark shifts, and so only the scalar components need be considered. The 674-nm ac Stark shift is negligible at the power level and beam waist size used in the trap. Although the 1092-nm and 422-nm beams are nominally switched off during the probe laser interrogation periods, in practice they are not perfectly extinguished. No significant frequency shift was detected between measurements carried out with and without an AOM switching the 1092-nm beam, setting a limit on the 1092-nm ac Stark shift under normal operating conditions from the measured extinction ratio of the AOM. Effective extinction of the 422-nm radiation is more important, because the cooling and probe transitions share the ground state as a common level. This beam is therefore blocked by using a combination of an AOM and a mechanical shutter, giving a total extinction ratio of 10^6. The residual 422-nm ac Stark shift due to light scattered around the shutter blade was determined by increasing the rf power leakage to the AOM by 15 dB, when it was nominally switched off, and scaling the frequency shift measured under these conditions to the normal leakage level.

Drifts in the ULE cavity frequency can lead to servo errors in the lock to the center of the Zeeman structure. To quantify this effect, we induced deliberate changes in both the magnitude and the direction of the cavity drift rate by adjusting the temperature control system, leading to larger-than-normal imbalances between the quantum jump rates on each side of the line. The relationship between measured frequency and quantum jump imbalance determined in this way was consistent with the relationship predicted on the basis of the observed linewidth and servo parameters. For the special case where measurements of the quantum jump rate are made at two frequencies separated by the linewidth of the Zeeman component, this relationship is given in (*21*).

The uncertainty in the maser reference frequency has contributions both from the

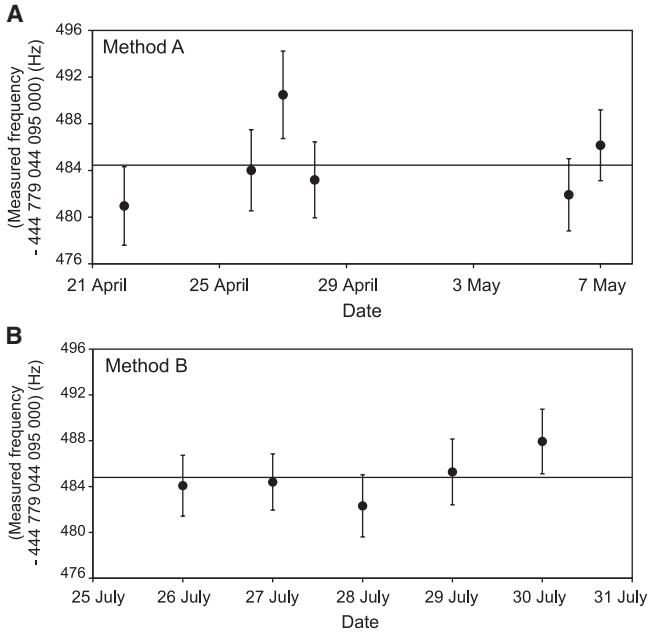

Fig. 2. Frequency of the $5s\ ^2S_{1/2}$–$4d\ ^2D_{5/2}$ transition in $^{88}Sr^{+}$, determined from (**A**) the average of measurements made in three nominally orthogonal magnetic field directions and (**B**) the average of measurements carried out by using three different pairs of Zeeman components corresponding to transitions for which $|m_j'| =$ 1/2, 3/2, and 5/2. The solid lines show the average measured value using each technique. Corrections have been applied for systematic frequency shifts as itemized in Table 1.

Table 1. Estimated size and standard uncertainty (Hz) of all systematic frequency shifts larger than 10 mHz.

Source	Method A		Method B	
	Shift	Uncertainty	Shift	Uncertainty
Quadrupole shift	0	0.5	0	<0.01
2nd-order Doppler shift due to micromotion	<0.01	0.01	<0.01	0.01
2nd-order Doppler shift due to secular motion	<0.01	0.01	<0.01	0.01
Stark shift due to micromotion	+0.01	0.01	+0.01	0.01
Stark shift due to secular motion	<0.01	0.01	<0.01	0.01
Blackbody Stark shift	+0.30	0.08	+0.30	0.08
1092-nm ac Stark shift	0	0.02	0	0.02
422-nm ac Stark shift	+1.4	0.8	+1.4	0.8
Servo errors	–1.0	0.6	–0.4	0.3
Maser reference frequency	0	0.7	0	0.7
Gravitational shift	0	0.1	0	0.1
Total estimated systematic shift	+0.7	1.3	+1.3	1.1

uncertainty in the Cs fountain frequency (1 part in 10^{15} statistical over the time scale of these measurements and 1 part in 10^{15} systematic) (*18*) and from the uncertainty in correcting for the frequency shifts in the cables used to transfer the maser signal to the femtosecond comb laboratory. Lastly, the uncertainty in the relative altitudes of the Sr ion trap and the Cs fountain leads to a small uncertainty because of the gravitational shift.

Correcting for the systematic shifts gives frequency values of 444,779,044,095,484.3 (1.9) Hz and 444,779,044,095,484.8 (1.6) Hz for the data taken with use of the two different methods of nulling the electric quadrupole shift, which agree to well within their statistical uncertainties. The unweighted mean of the two values gives a final value for the 674-nm electric quadrupole clock transition frequency in $^{88}Sr^{+}$ of 444,779,044,095,484.6 (1.5) Hz. In calculating the final uncertainty, only the statistical error is reduced, because the systematic uncertainties are mostly common to the two measurements. This result is in good agreement with earlier, less-accurate measurements (*9*, *10*) of the Sr clock transition frequency. It is also a factor of 3 more accurate than any previously reported optical frequency measurement, and its fractional uncertainty of 3.4×10^{-15} is within a factor of 3 of that of the NPL primary Cs standard (when both statistical and systematic errors are considered). Apart from the uncertainty arising from the Cs standard, the dominant sources of uncertainty in our measurement are technical in nature and can be reduced by refinements to the experimental arrangement. In particular, improvements to the extinction of the cooling laser radiation during the probe laser periods (e.g., by placing an iris after the shutter) will reduce the 422-nm ac Stark shift, whereas reductions in the probe laser linewidth and ULE cavity drift rate will reduce servo errors. A second endcap trap is also being developed, which will enable a more detailed investigation of systematic errors by means of two-trap comparisons. With these improvements, we anticipate a frequency measurement that is limited by the accuracy of the Cs fountain. As well as being of interest for a possible future redefinition of the second, measurements of this and other optical frequency standards over timescales of a few years will provide increasingly sensitive laboratory tests of the time invariance of fundamental constants (*22*, *23*).

References and Notes

1. P. Gill, Ed., *Proceedings of the 6th Symposium on Frequency Standards and Metrology* (World Scientific, Singapore, 2002).
2. R. J. Rafac *et al.*, *Phys. Rev. Lett.* **85**, 2462 (2000).
3. S. A. Diddams *et al.*, *Science* **293**, 825 (2001); published online 12 July 2001 (10.1126/science.1061171).
4. T. Udem, J. Reichert, R. Holzwarth, T. W. Hänsch, *Opt. Lett.* **24**, 881 (1999).
5. S. A. Diddams *et al.*, *Phys. Rev. Lett.* **84**, 5102 (2000).
6. J. Stenger, C. Tamm, N. Haverkamp, S. Weyers, H. R. Telle, *Opt. Lett.* **26**, 1589 (2001).
7. P. J. Blythe *et al.*, *Phys. Rev. A* **67**, 020501(R) (2003).
8. T. Becker *et al.*, *Phys. Rev. A* **63**, 051802(R) (2001).
9. H. S. Margolis *et al.*, *Phys. Rev. A* **67**, 032501 (2003).
10. A. A. Madej, J. E. Bernard, P. Dubé, L. Marmet, R. S. Windeler, *Phys. Rev. A* **70**, 012507 (2004).
11. T. Udem *et al.*, *Phys. Rev. Lett.* **86**, 4996 (2001).
12. C. A. Schrama, E. Peik, W. W. Smith, H. Walther, *Opt. Commun.* **101**, 32 (1993).
13. I. Siemers, M. Schubert, R. Blatt, W. Neuhauser, P. E. Toschek, *Europhys. Lett.* **18**, 139 (1992).
14. D. J. Berkeland, J. D. Miller, J. C. Bergquist, W. M. Itano, D. J. Wineland, *J. Appl. Phys.* **83**, 5025 (1998).
15. R. W. P. Drever *et al.*, *Appl. Phys. B* **31**, 97 (1983).
16. H. Dehmelt, *IEEE Trans. Instrum. Meas.* **31**, 83 (1982).
17. G. P. Barwood, H. S. Margolis, G. Huang, P. Gill, H. A. Klein, *Phys. Rev. Lett.* **93**, 133001 (2004).
18. K. Szymaniec, W. Chalupczak, P. B. Whibberley, S. N. Lea, D. Henderson, in preparation.
19. W. M. Itano, *J. Res. Natl. Inst. Stand. Technol.* **105**, 829 (2000).
20. P. Dubé, L. Marmet, A. A. Madej, J. E. Bernard, presentation at the 2004 Conference on Precision Electromagnetic Measurements, London, 27 June to 2 July 2004.
21. J. E. Bernard, L. Marmet, A. A. Madej, *Opt. Commun.* **150**, 170 (1998).
22. M. Fischer *et al.*, *Phys. Rev. Lett.* **92**, 230802 (2004).
23. E. Peik *et al.*, *Phys. Rev. Lett.* **93**, 170801 (2004).

24. We thank W. Chalupczak, D. Henderson, P. Stacey, and P. Whibberley for their contributions to the caesium fountain and hydrogen maser operation. This work was supported by the Department of Trade and Industry National Measurement System Length program under contract LE02/A01.

21 September 2004; accepted 25 October 2004

Multifunctional Carbon Nanotube Yarns by Downsizing an Ancient Technology

Mei Zhang,[1] Ken R. Atkinson,[2] Ray H. Baughman[1]*

By introducing twist during spinning of multiwalled carbon nanotubes from nanotube forests to make multi-ply, torque-stabilized yarns, we achieve yarn strengths greater than 460 megapascals. These yarns deform hysteretically over large strain ranges, reversibly providing up to 48% energy damping, and are nearly as tough as fibers used for bulletproof vests. Unlike ordinary fibers and yarns, these nanotube yarns are not degraded in strength by overhand knotting. They also retain their strength and flexibility after heating in air at 450°C for an hour or when immersed in liquid nitrogen. High creep resistance and high electrical conductivity are observed and are retained after polymer infiltration, which substantially increases yarn strength.

Archaeological evidence from the late Stone Age indicates that humans long ago discovered the basic secrets of spinning (*1*). Similar processes involving the twisting of centimeter-long fibers to make continuous yarns are critically important for many of today's industries, and they remain a focus of research and development. The present work reduces the diameters of fibers used for spinning by a factor of 1000, increases twist by about the same factor, and discovers useful properties for the resulting spun carbon nanotube yarns.

Nanotube spinning is motivated in part by interest in the very high strength and electrical and thermal conductivities of individual nanotubes (*2*). Breakthroughs have been made in wet spinning of single-walled nanotubes (SWNTs) (*3*–*6*) and in dry-state spinning of multiwalled nanotubes (MWNTs) and SWNTs (*7*, *8*), but the highest strength achieved with any of these spinning methods is about an order of magnitude lower than the strength of individual SWNTs, ~37 GPa (*2*).

There is no single best solution to the challenge of converting available nanotube powders into useful fibers and yarns. Excellent fiber strength (4.2 GPa) and modulus (167 GPa) have been achieved by incorporating SWNTs in a high-strength, high-modulus polymer, but electrical and thermal conductivities are low because of limitations on nanotube content (*5*). Much higher conductivities result for thermally annealed, solution-spun yarns comprising only SWNTs (*2*, *4*), but achieved mechanical properties are far lower than can be obtained using a polymer matrix for intertube stress transfer (*6*). Coagulation-spun yarns comprising ~60 weight % SWNTs in a polymer matrix have high strength (~1.8 GPa) and more than 10 times the toughness (~600 J/g) of any synthetic polymer, but the electrical conductivity is so low that charge/discharge rates for fiber-based supercapacitors are limited (*6*). The challenge is to produce yarns that are at the same time strong, creep resistant, highly

[1]NanoTech Institute and Department of Chemistry, University of Texas at Dallas, Richardson, TX 75083, USA. [2]CSIRO Textile & Fibre Technology, P.O. Box 21, Belmont, Victoria 3216, Australia.

*To whom correspondence should be addressed. E-mail: ray.baughman@utdallas.edu